Journal of Experimental Nanoscience
Publication details, including instructions for authors and subscription information:
http://www.informaworld.com/smpp/title~content=t716100757

Synthesis, characterization and catalytic activity of metal nanoparticles in the selective oxidation of olefins in the gas phase

R. J. Chimentão[a]; N. Barrabés[a]; F. Medina[a]; J. L. G. Fierro[b]; J. E. Sueiras[a]; Y. Cesteros[c]; P. Salagre[c]
[a] Department d'Enginyeria Química, Universitat Rovira i Virgili, Tarragona, Spain [b] Instituto de Catalisis y Petroleoquimica, CSIC, Madrid, Spain [c] Department de Química Inorgánica, Universitat Rovira i Virgili, Tarragona, Spain

To cite this Article Chimentão, R. J. , Barrabés, N. , Medina, F. , Fierro, J. L. G. , Sueiras, J. E. , Cesteros, Y. and Salagre, P.(2006) 'Synthesis, characterization and catalytic activity of metal nanoparticles in the selective oxidation of olefins in the gas phase', Journal of Experimental Nanoscience, 1: 4, 399 — 418
To link to this Article: DOI: 10.1080/17458080601024196
URL: http://dx.doi.org/10.1080/17458080601024196

Journal of Experimental Nanoscience,
Vol. 1, No. 4, December 2006, 399–418

Taylor & Francis
Taylor & Francis Group

Synthesis, characterization and catalytic activity of metal nanoparticles in the selective oxidation of olefins in the gas phase

R. J. CHIMENTÃO†, N BARRABÉS†, F. MEDINA*†, J. L. G. FIERRO‡, J. E. SUEIRAS†, Y. CESTEROS§ and P. SALAGRE§

†Department d'Enginyeria Química, Universitat Rovira i Virgili, 43007, Tarragona, Spain
‡Instituto de Catalisis y Petroleoquimica, CSIC, Cantoblanco, 28049, Madrid, Spain
§Department de Química Inorgánica, Universitat Rovira i Virgili, 43005, Tarragona, Spain

(*Received August 2006; in final form September 2006*)

Shape controlled metal nanoparticles were studied in the epoxidation of olefins. PVP mediated polyol processes were employed to generate silver nanowires/rods, nanocubes and nanopolyhedra. Spherical copper nanoparticles were also obtained by the polyol process. The mean diameter of the silver nanoparticles was around 150 nm. Furthermore, Cu nanoparticles were synthesized in an ethanol solution using CTAB as surfactant and as reducing agent. Additionally Au nanoparticles were synthesized by a phase-transfer system irradiated with 254 nm UV light. The mean diameter of these Au and Cu nanoparticles was around 10 nm. The catalytic activity of these nanoparticles on several supports such as α-Al_2O_3, $CaCO_3$ and spherical particles of TiO_2 obtained by the Stöber method was investigated in the epoxidation of a no-allylic olefin such as styrene, as well as for an allylic olefin, such as propene, using molecular oxygen and N_2O as oxidants. The effect of Cs promotion in the styrene epoxidation was also investigated. The type of metal, the particle size, the support and the oxidant, as well as the addition of promoters such as Cs, showed a strong influence towards the formation of selective oxidation products. The metal nanoparticles were characterized employing various techniques such as X-ray diffraction (XRD), temperature programmed reduction (TPR), UV-visible spectroscopy, transmission electron microscopy (TEM), scanning electron microscopy (SEM), X-ray photoelectron spectroscopy (XPS) and ICP-AES.

Keywords: Copper; Epoxidation; Gold; Nanocubes; Nanoparticles; Nanopolyedra; Nanowires; Olefins; SEM; Silver; TEM; UV-vis

1. Introduction

The development of uniform nanometre sized particles has been intensively pursued because of the many technological and fundamental scientific interests associated with these nanoparticles [1]. Nanoscales materials such as metal nanoparticles have received great attention due to their potential applications in the areas of nanofabrication,

*Corresponding author. Email: francesc.medina@urv.cat

Journal of Experimental Nanoscience
ISSN 1745–8080 print/ISSN 1745–8099 online
http://www.tandf.co.uk/journals
DOI: 10.1080/17458080601024196

optoeletronic nanodevices and biological nanosensors [2]. In recent years, most of the investigations have been focused on the control of the shape and size of the nanoparticles [3]. The formation of monosized metallic nanoparticles is achieved in most cases by a combination of a low concentration of solute and polymeric monolayer adhered onto the growth surfaces. Metal nanowires/rods have been synthesized by various methods such as templating [4, 5], photochemistry [6], seeding [7, 8] and electrochemistry [9, 10]. The various synthesis methods or techniques can be grouped into two categories: the thermodynamic equilibrium approach and the kinetic approach. In the thermodynamic approach, the synthesis process consists of (i) generation of supersaturation, (ii) nucleation, and (iii) subsequent growth. In the kinetic approach, the formation of nanoparticles is achieved by either limiting the amount of precursors available for the growth such as used in molecular beam epitaxy, or confining the growth in a limited space such as aerosol synthesis or micelle synthesis. In this work, attention will be focused on both synthesis approaches.

Here the synthesis of nanoparticles through the thermodynamic approach was based on the polyol process [11], leading the formation of monosized metallic particles such as nanowires, nanocubes and nanopolyhedra of silver and copper nanospheres. Ethylene glycol has been widely used in this synthesis process due to its strong reducing power and relatively high boiling point [12], whereas the anisotropy growth of the nanoparticles is controlled by the presence of stabilizers such as PVP. For the formation of nanowires or nanorods, anisotropic growth is required; i.e. the crystal grows along a certain orientation faster than others.

For the kinetic approach we synthesized gold nanoparticles by kinetically confining the reaction in a restricted space. This method is exemplified by the synthesis of nanoparticles inside micelles or in microemulsion. When the surfactant or block polymers that typically consist of two parts, one hydrophilic and another hydrophobic, are dissolved in a solvent they preferentially self-assemble in hydrocarbon/aqueous solution in such way as to form micelles [13]. In micelle synthesis, reactions precede among the reactants that are available only inside the micelle and the particle stops growing when the reactants are consumed [14].

Using these protocols, several, silver, gold and copper nanoparticles with different particle sizes and morphologies were synthesized. Then, the obtained metal nanoparticles were supported on α-Al_2O_3, $CaCO_3$, TiO_2 and spheres of TiO_2 (both in anatase crystalline form). The procedures for the preparation of titania spheres were simple and straightforward. The method is similar to that reported by Stöber and coworkers for the synthesis of SiO_2 spheres [15].

The catalytic activity of the as-synthesized metal nanoparticles was studied in the epoxidation of olefins such as styrene and propene in gas phase. The epoxidation of olefins is an extremely important catalytic reaction in the chemical industry [16]. The silver supported on α-Al_2O_3 catalysed gas phase epoxidation of ethylene using molecular oxygen is one of the most successful examples of heterogeneous catalysis to date [17]. However, more efforts to directly epoxidize other olefins, such as propene, to their corresponding epoxides using molecular oxygen in a commercially viable process are necessary. The lower selectivity obtained for propene epoxidation instead of for ethylene has been attributed to a greater reactivity of the allylic hydrogen in propene compared to that of the vinyl hydrogen in ethylene [18]. However, Haruta and

coworkers have reported that a feed stream consisting of C_3H_6, O_2 and H_2 can be selectively epoxidized to form propene oxide using highly dispersed gold supported on TiO_2 [19]. It seems that the size of the gold particle plays an important role in the selective oxidation reaction of propene in gas phase. An alternative oxidizing agent for the epoxidation of propene is nitrous oxide (N_2O). This oxidant has received much attention for many different oxidation reactions especially after the discovery that selective oxidation of benzene to phenol by nitrous oxide could be performed over Fe-ZSM-5 zeolite [20]. Nitrous oxide has certain properties which generate a mild electrophilic peroxide-like oxygen species, and a nucleophilic one as well. Energetically, the release of an oxygen atom from N_2O is more favourable than from an oxygen molecule [21]. However, the catalyst for the epoxidation of propene must adsorb and activate the N_2O molecule without decomposing it [22].

In this account, we report the synthesis of shape control of several metal nanoparticles and their applications in the selective oxidation of styrene and propene in the gas phase using molecular oxygen and N_2O as oxidants. In addition, the cesium promotion effect over silver nanoparticle in styrene epoxidation was also studied. The samples were characterized using temperature programmed reduction (TPR), X-ray photoelectron spectroscopy (XPS), X-ray diffraction (XRD), scanning electron microscopy (SEM), transmission electron microscopy (TEM), ICP-AES, UV-visible absorption spectra and selected area electron diffraction pattern (SAED) in order to correlate the morphological dependence of metal particles with the catalytic behaviour.

2. Experimental

2.1. *Preparation of the silver nanoparticles*

Silver nanowire catalysts were prepared by the polyol process. In a typical synthesis of silver nanoparticles, 30 ml ethylene glycol solution of $AgNO_3$ (0.25 M, Aldrich) and 30 ml ethylene glycol (EG) solution of polyvinyl-pyrrolidone (PVP) (0.375 M in repeating unit weight-average molecular weight ≈40,000, Aldrich) were simultaneously added in 50 ml ethylene glycol at 433 K under vigorous magnetic stirring. The reaction mixture was then refluxed for 45 min at this temperature. The obtained nanoparticles were diluted with acetone and separated from ethylene glycol (EG) by centrifugation at 4000 rpm for 20 min. Then, silver nanowires (11 wt.%) were dispersed by impregnation on α-Al_2O_3 with an acetone solution. We also synthesized silver nanoparticles with $AgNO_3$/PVP molar ratio of 3. The α-Al_2O_3 support (0.4 m^2/g) was calcined at 673 K for 4 h before use. For comparison $CaCO_3$ support (20 m^2/g) was also employed. These samples were proved in the styrene epoxidation. Silver nanowires (1 wt.%) were also supported in TiO_2 (anatase) and studied in the propene epoxidation reaction. The procedure for catalyst activation, before the characterization and the activity tests, involved heating up to a temperature of 623 K in O_2 flow (heating rate 2 K/min), and then reduced in H_2 flow up to a temperature of 623 K (heating rate 5 K/min) at atmospheric pressure, followed by isothermal reduction at this temperature for 3 h. To investigate the promotion effect by cesium the catalysts were impregnated by an aqueous solution containing appropriate amounts of CsOH. After that the promoted catalyst was activated using the same protocol.

2.2. *Preparation of the copper nanoparticles*

The copper nanoparticles were prepared by two procedures (A and B). First, in procedure A, the copper nanoparticles were synthesized following the same approach described for the silver nanoparticles in the polyol process. Copper nanospheres were obtained and then dispersed by impregnation (11 wt.%) on α-Al_2O_3 and (1 wt.%) TiO_2 with an acetone solution. These catalysts were studied in the epoxidation of styrene and propene, respectively. Here the same activation procedure for the silver catalyst was employed.

In the second procedure (B), an ethanol solution of $Cu(NO_3)_2 \cdot 6H_2O$ (1 ml, 5 mM) was mixed with an ethanol solution of cetyltrimethylamonium bromide (CTAB, 1 ml, 5 mM) in a 25 ml flask. The flask was immersed in an ice bath, and the solution was bubbled with Ar under constant stirring for ~30 minutes. The blue colour of the copper solution turned orange. These copper nanoparticles were supported (1 wt.%) on TiO_2 spheres to study the propene epoxidation reaction.

2.3. *Synthesis of TiO_2 spheres*

Monodispersed TiO_2 microspheres were synthesized by the Stöber method [15]. In a typical preparation, 50 ml of NH_4OH was mixed with ethanol (320 ml). Then 16 ml of tetraorthotitanate (TEOT) was added dropwise to the above solution. The resultant solution was stirred for 4 h, and then the white precipitate was filtered. The product was repeatedly washed with ethanol and then dried at 373 K for 4 h in order to remove the water and solvents, and finally calcined at 623 K for 4 h in a muffle furnace.

2.4. *Synthesis of gold nanoparticles*

Gold nanoparticles were synthesized in a toluene/water system at room temperature [23]. Aqueous solution of gold metal ions was mixed with toluene solution containing hexadecylamine ($C_{16}H_{33}NH_2$) under vigorous stirring. An immediate two-layer separation was produced, with an orange red organic phase on the top and an orange tinted aqueous phase on the bottom. The resulting solution was stirred for 48 h protected from the light. At the end of the process a deep yellow toluene phase containing the $AuCl_4^-$ ions was in equilibrium with a colourless aqueous phase. Finally, the organic phase containing the gold ions was removed from the aqueous phase. Then, the gold solution was irradiated for 40 h with a 254 nm UV light (2000 $\mu W/cm^2$) for about 40 h. The resultant red wine toluene solution of gold nanoparticles was deposited (1 wt.%) on the TiO_2 spheres. The solvent was evaporated slowly and the samples were then calcined in air (623 K) to remove the amine ligands. The catalysts were characterized for their gold content by ICP-AES (using Perkin–Elmer Analyser).

2.5. *Catalyst characterization*

2.5.1. X-ray diffraction (XRD). XRD measurements were made using a Siemens D5000 diffractometer (Bragg-Bentano parafocusing geometry and vertical θ–θ goniometer) fitted with a curved graphite diffracted-beam monochromator, incident and diffracted beam Soller slits, a 0.06° receiving slit and scintillation counter as detector.

The angular 2θ diffraction range was between 30° and 90°. The data were collected with an angular step of 0.05° at 3 s per step and sample rotation. $Cu_{K\alpha}$ radiation was obtained from a copper X-ray tube operated at 40 kV and 30 mA.

2.5.2. Scanning electron microscopy (SEM). The morphologies of the catalysts were observed by SEM with a JEOL JSM-35C scanning microscope operated at an acceleration voltage of 15 kV. A small portion of each sample powder was coated on a metallic disk holder and covered with a thin gold layer before the SEM analysis.

2.5.3. Transmission electron microscopy (TEM). Transmission electron micrographs were taken of the samples using a JEOL-2010 electronic microscope operating at an accelerating voltage of 200 kV. Samples for TEM were prepared by depositing the sample on the copper grid and then the solvent was allowed to evaporate under vacuum before analysis.

2.5.4. UV-vis spectroscopy (UV-vis). UV-vis spectra of the silver–gold solution were carried out at ambient temperature using a HP 8542 spectrophotometer by scanning wavelengths between 300 and 820 nm.

2.5.5. Temperature-programmed reduction (TPR). TPR experiments were performed in a TPDRO 1100 (Thermo Finnigan), equipped with a thermal conductivity detector (TCD) and coupled to a mass spectrometer QMS 422 Omnistar. The catalysts were treated in O_2 for 1 h at 623 K before TPR analysis. Then, the samples were purged with argon flow before the TPR analysis. The TPR was carried out using 5% H_2 in Ar flow as reducing agent, and the gas flow rate was 20 ml/min. The gases evolved during the TPR experiment were monitored by TCD and mass spectrometer detector. The temperature was raised from 323 K up to 1073 K at a rate of $\beta = 20$ K/min. Water produced during TPR was trapped in $CaO + Na_2O$ (Soda lime).

2.5.6. X-ray photoelectron spectroscopy (XPS). The XPS spectra were acquired in a VG Escalab 200R electron spectrometer equipped with a hemispherical electron analyser, operating in a constant pass energy mode, and a non-monochromatic Mg-Kα ($h\nu = 1253.6$ eV, 1 eV $= 1.603 \times 10^{-19}$ J). The X-ray source operated at 10 mA and 12 kV. The background pressure in the analysis chamber was kept below 7×10^{-9} mbar during data acquisition. The binding energy (BE C1s = 284.9 eV) of adventitious C_1 was used as reference. A Shirley background subtraction was applied and Gaussian–Lorentzian product functions were used to approximate the line shapes of the fitting components.

2.6. *Catalytic activity*

2.6.1. Styrene epoxidation. The catalytic epoxidation of styrene was performed in a stainless steel tubular down-flow reactor. The size of the fix-bed reactor was Ø10 mm × 20 cm long provided with a temperature control system. The reaction temperature was measured in the middle of the catalyst bed by means

of a K-type thermocouple. The reactor was filled with the catalyst (1.0 g), which had been previously ground and sieved in the range of 75–100 mesh. The reactor was placed in an electric furnace with a temperature control system. A pressure indicator was used to measure the pressure drop in the catalyst bed. Catalytic activity was measured at steady state conditions (after 5 hours of time on stream). The feedstock gas, consisting of a mixture of O_2–Ar, was fed to the reactor by independent mass flow controllers, using a total flow rate between 100 and 300 ml/min. The styrene was introduced into the reactor by a high-pressure metering pump, which worked in a flow-rate range of 0.1–1.0 ml/h. The reaction temperature was 573 K working at atmospheric pressure. The effluent gas was rapidly cooled and analysed off-line using a Shimadzu GC 2010 gas-chromatograph equipped with an Ultra 2 capillary column and flame ionization detector (FID). The presence of combustion products was determined by on-line TCD and mass spectrometer.

2.6.2. Propene epoxidation. A flow reactor was used to determine the catalytic performance. The experiments were carried out with typically 0.14 g of catalyst and a gas flow of 50 N ml min^{-1} (GHSV 9000 h^{-1}). The gas mixture consisted of 10% of N_2O or O_2, 10% of H_2 and 10% propene in argon. The catalytic reactions were carried out using a fixed-bed reactor operated at atmosphere pressure. The catalyst was pretreated with gas flow containing Ar (100 ml min^{-1}) and H_2 (10 ml min^{-1}) at 823 K for 1 h. After the temperature was decreased to the desired reaction temperature, the reactant gas mixture of Ar, C_3H_6, N_2O or O_2 and H_2 was introduced to start the reaction. The products were analysed by two on-line gas chromatographs equipped with Porapak T and molecular sieves columns using FID and TCD detectors. All the lines and valves between the exit of the reactor and the gas chromatographs were heated to 373 K to prevent the condensation of the products.

3. Results and discussion

3.1. *Ag and Cu nanoparticles prepared by the polyol process*

At elevated temperatures, ethylene glycol can reduce Ag^+ ions into Ag atoms, and thereby induce the nucleation and growth of silver nanostructures in the solution phase. On the basis of the reaction of silver nitrate and PVP in EG at 433 K, once the solutions of $AgNO_3$ and PVP had been introduced to the reaction system, a bright yellow colour gradually appeared indicating the formation of silver nanoparticles through the reduction of $AgNO_3$ with ethylene glycol [24]. At the end of the process the silver solution was grey. The silver nanoparticles were diluted in acetone and separated from the ethylene glycol and PVP by centrifugation. It was found that the morphology of the silver particles was significantly influenced by the $AgNO_3$/PVP molar ratio, temperature and the time on reflux. Figure 1(a)–(c) shows the silver nanoparticles obtained from the polyol process supported on α-Al_2O_3. The diameters of the silver nanoparticles were reasonably uniform with an average value of 150 nm. When the $AgNO_3$/PVP molar ratio was 1.5 the product was dominated by silver nanowires. An SEM image of the as-synthesized silver nanowires supported on α-Al_2O_3

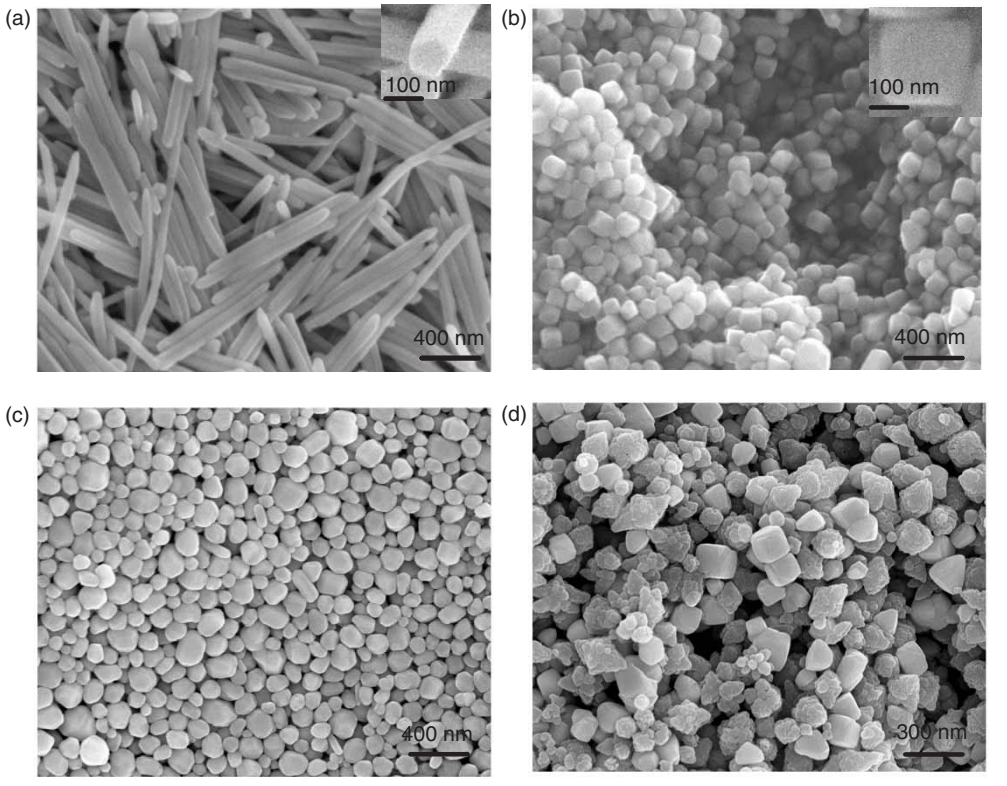

Figure 1. SEM image of the as-prepared by polyol process of the silver nanoparticle catalyst supported on α-Al_2O_3 (a) silver nanowires, (b) silver nanocubes, (c) silver nanopolyhedra and (d) silver nanocubes supported on $CaCO_3$.

(11% $Ag^{(NW)}/\alpha$-Al_2O_3) is depicted in figure 1(a). The inset of figure 1(a) shows that the cross-section of the silver nanowires clearly has a pentagonal shape which is in agreement with previous results [25]. When this molar ratio increased from 1.5 to 3 truncated silver nanocubes where generated as shown in figure 1(b). Silver nanopolyhedra were also obtained when the silver nanocubes were maintained for a longer period of time in the reaction mixture. Figure 1(c) shows the SEM image of the silver nanopolyhedra catalyst (11% $Ag^{(NP)}/\alpha$-Al_2O_3). Figure 1(d) shows the silver nanocubes catalysts (11% $Ag^{(NC)}/CaCO_3$) supported on $CaCO_3$, (calcite, JCPDS file 14 24-27A). No silver nanoparticles were obtained by the polyol process at temperatures lower than 433 K.

X-ray diffraction (XRD) taken from these silver nanoparticles (figure 2) revealed the presence of pure silver showing three diffraction peaks which are assigned to (111), (200) and (220) reflections of the face centred cubic structure (fcc) of silver (JCPDS file 04-0783). Figure 2(a)–(c) shows the XRD patterns from silver nanocubes, nanopolyhedra and nanowires, respectively. As shown in figure 2, the XRD pattern showed sharp reflections corresponding to the face-centred cubic structure of metallic silver. The (111) reflection was intensified considerably indicating that the surface of silver nanoparticles is oriented in this plane. The anisotrophic growth was maintained by selectively

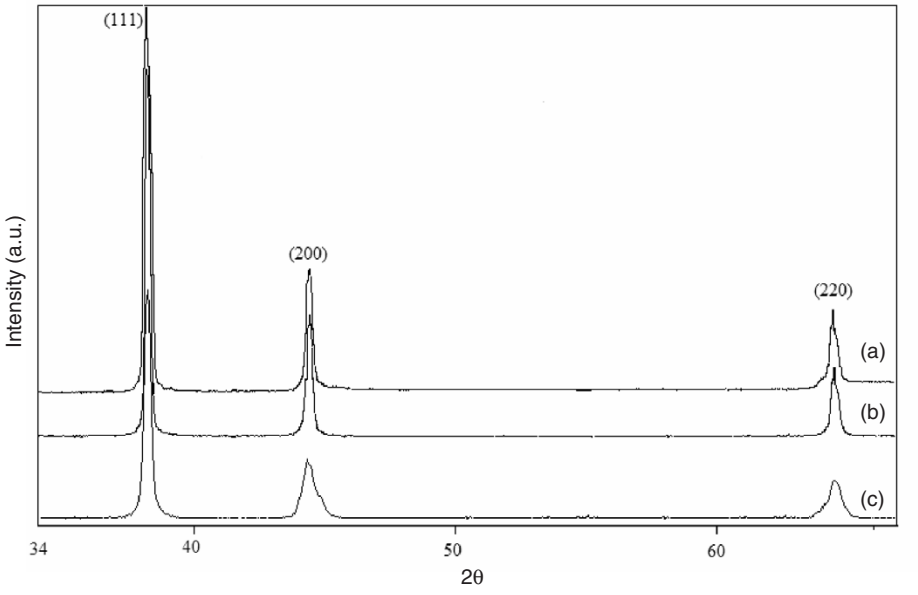

Figure 2. Corresponding XRD patterns of the as-synthesized Ag nanostructures by polyol process, (a) nanocubes, (b) nanopolyhedra and (c) Ag nanowires.

covering the (100) facets with PVP while leaving the (III) facets largely uncovered by PVP and thus highly reactive. On the basis of energetic considerations, the optimal particle shape for the fcc metal is a truncated octahedron with regular hexagonal faces. It has been proposed that the different interaction between PVP and various crystalline facets leads to anisotropic growth of Ag nuclei and further to the formation of different shaped Ag nanostructures [26]. In general, a silver single crystal has a face-centred cubic (fcc) structure, therefore the pentagonal shape of the cross-sections observed for our silver nanowires indicates a multiple twinned structure. It becomes clear that these silver nanostructures tend to grow as bicrystals twinned along the (111) planes, showing (111) crystal faces at their surface [27].

Figure 3 shows an XRD pattern of the copper particles prepared by the polyol process (procedure A). The product exhibits a high crystallinity no detecting other phases such as copper oxide (CuO) and cuprous oxide (Cu_2O). Typical XRD pattern at $2\theta = 43.4^\circ$, 50.6° and 74.2° that are indexed as (111), (200) and (220) planes of the fcc structure of copper was obtained (corresponding to the JCPDS file, 4–386). Copper nanospheres were obtained by the polyol process with an average particle size of around 350 nm. The inset of figure 3 shows the SEM image of the spherical copper nanoparticles supported on α-Al_2O_3 (11% $Cu^{(NS)}/\alpha$-Al_2O_3).

3.2. *Synthesis of Au nanoparticles by phase transfer and Cu nanoparticles by procedure B*

The resultant stabilized colloidal gold in toluene was in turn characterized by TEM, SAED and UV-vis. Figure 4 shows the TEM images of these gold nanoparticles.

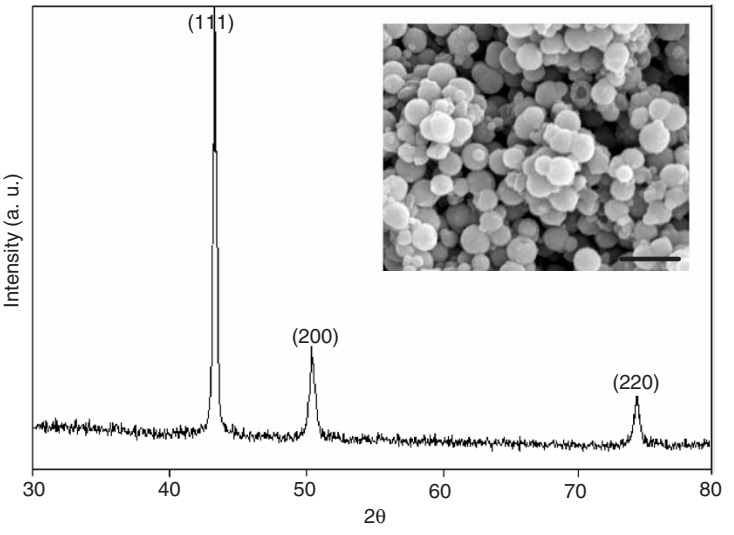

Figure 3. XRD pattern of the Cu nanoparticles synthesized by the polyol process. Inset: TEM image of the corresponding Cu nanoparticles. The corresponding scale bar is 700 nm.

The particle size was around 10 nm showing the reliability of the two-phase procedure for the preparation of colloidal gold nanoparticles. The inset of figure 4 gives the selected area electron diffraction (SAED) pattern obtained from these gold nanoparticles. All the diffraction rings can be assigned to pure fcc of gold with a lattice constant of 4.0709 Å (4.0786 Å in JCPDS file 04-0784). The surface analysis of these gold nanoparticles was evaluated by X-ray photoelectron spectroscopy (XPS). The corresponding XPS core-level spectra of the Au-4*f* region acquired for these gold nanoparticles sample is depicted in figure 5(b). The Au-4*f* spectra, characterized by the spin–orbit splitting (Au $4f_{7/2}$ and Au $4f_{5/2}$ components), shows values of 84.0 and 87.7 eV, respectively. There is no evidence that the Au was bound to oxygen because the oxide shows binding energies around 85.5 and 89.5 for Au $4f_{7/2}$ and Au $4f_{5/2}$, respectively. Both peaks indicate that these binding energies are consistent with Au^0 oxidation state [28, 29]. UV-vis spectroscopy exhibits the characteristic surface plasmon absorption band of colloidal nanoparticle appearing at 525 nm as shown in the figure 5(b). Due to their surface plasmon vibration the gold nanoparticles have a characteristic absorption in the visible region of the electromagnetic spectrum at around 500–600 nm, which is responsible for the striking violet-to-pink range of colours of the nanoparticles, depending of the particle size [30]. The inset of figure 5(b) shows a picture of our toluene solution of gold taken at the end of the UV light irradiation period (40 h) showing a red wine colour. It has been reported [31] that the origin of this absorption is from the plasmon effect of the gold particles. It originates from the collective oscillations of the electrons at the surface of the nanoparticles, and therefore is affected by the particle size. It is noteworthy that the wavelength of the UV light irradiation controls the particle size but this fact is not a result of the photothermal effect [32]. The results reported here provide clear evidence for the importance of plasmon excitation in the Au nanoparticle reduction and growth process.

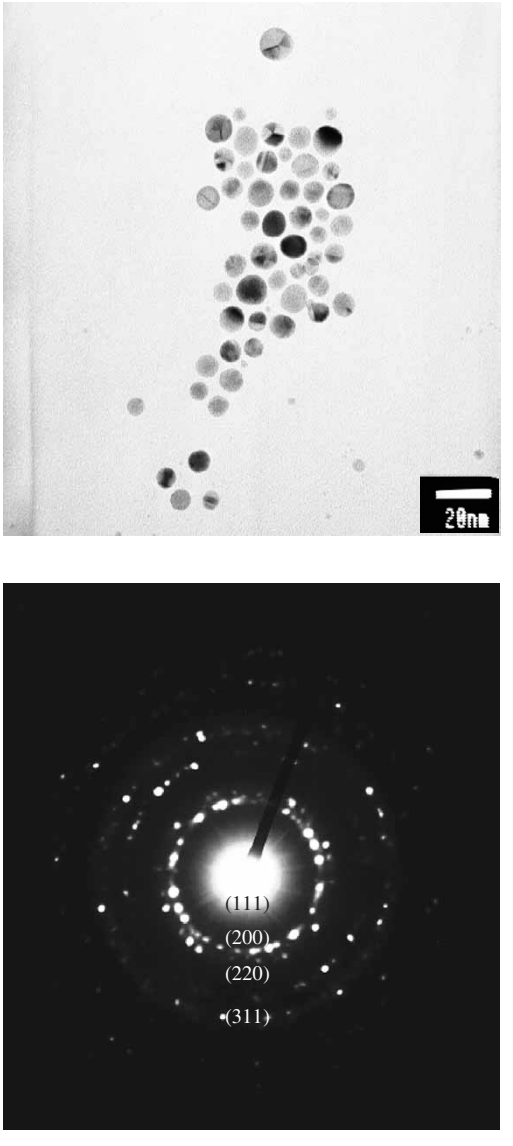

Figure 4. TEM image of gold nanoparticles after 40 h of irradiation with UV light. Inset: The selected area diffraction pattern (SAED) taken from these Au nanoparticles.

Figure 6 shows the UV-vis absorption spectra of the copper nanoparticles obtained by procedure B. The spectra show a characteristic absorption band of Cu at 520 nm. Moreover, the characteristic absorption band for copper oxide around 800 nm [33] was not observed. The TEM image of copper nanoparticles prepared by the procedure B is depicted in the inset of figure 6 as well as the picture of the resultant copper nanoparticle solution after the synthesis showing an orange colour. The TEM images show spherical copper nanoparticles with particle sizes around 10 nm.

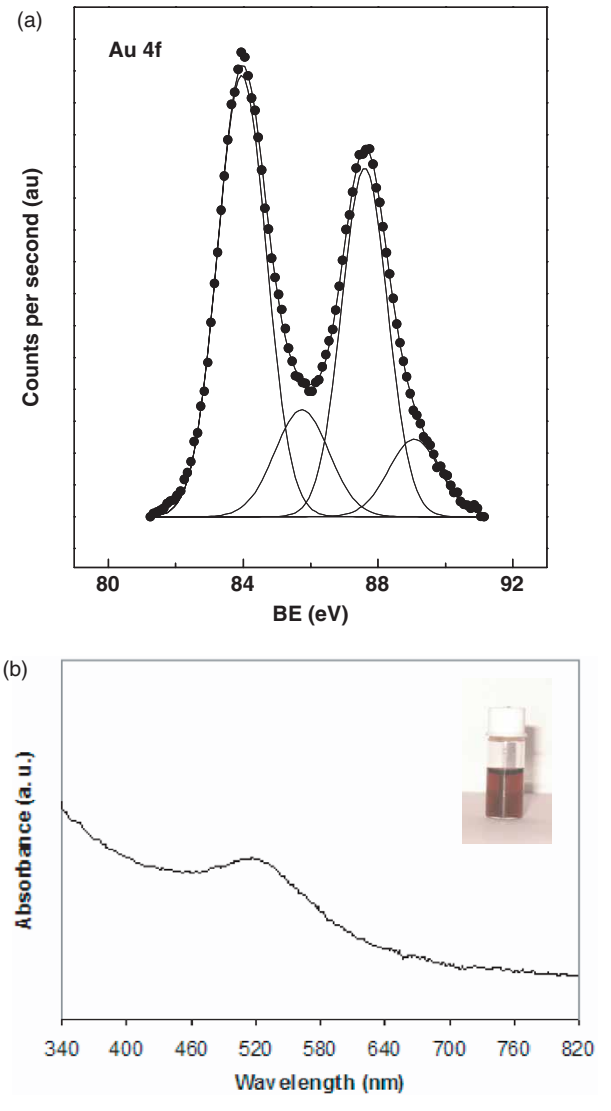

Figure 5. (a) Corresponding XPS analysis of the gold after photoinduction period. (b) UV-vis spectrum taken from the toluene solution containing the gold nanoparticles. Inset: Picture of photoinduced prepared gold nanoparticles solution showing the red wine colour.

3.3. *Ag and Cu nanoparticle catalyst characterization and catalytic activity in the styrene epoxidation*

The reducibility of silver nanowire catalysts as well as the effect of the addition of cesium was studied by TPR (figure 7a, b). Two oxygen peaks were observed over pure silver nanowire catalysts. The unpromoted silver nanowire catalyst shows two broad peaks at around 633 K (the most intense peak) and 873 K as depicted in figure 7(a). Previous studies of oxygen adsorption on silver have attempted to characterize the

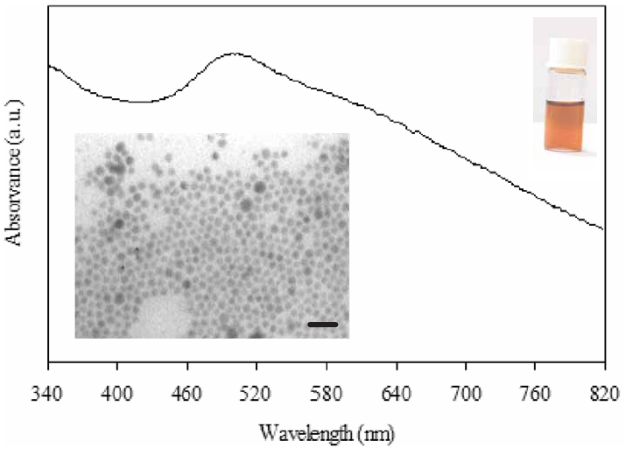

Figure 6. UV-vis spectrum taken from the ethanol solution containing copper nanoparticles. Inset: Picture of as-synthesized copper nanoparticles solution showing the orange colour and the TEM image of the corresponding Cu nanoparticles. The scale bar is 30 nm.

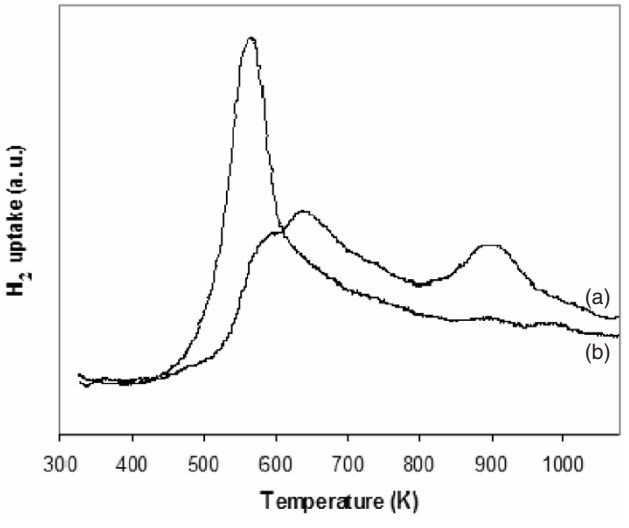

Figure 7. Temperature programmed reduction profiles (TPR). (a) Unpromoted silver nanowire catalyst ($11\%Ag^{(NW)}/\alpha\text{-}Al_2O_3$). (b) Cesium promoted silver nanowire catalyst ($11\%Ag^{(NW-0.25\%Cs)}/\alpha\text{-}Al_2O_3$) catalyst.

nature of the adsorbed species. The peak around 600 K has been attributed to the presence of subsurface oxygen (O_β) [34–40]. The presence of reduction peaks at higher temperatures can be attributed to the presence of oxygen species that are strongly chemisorbed on the surface of silver and are labelled as (O_γ) [37, 41–43]. The influence of the addition of cesium on the reducibility of silver nanowire catalyst (11% $Ag^{(NW)}/\alpha\text{-}Al_2O_3$) is illustrated in figure 7(b). Practically one main peak is observed for cesium promoted silver nanowire catalysts.

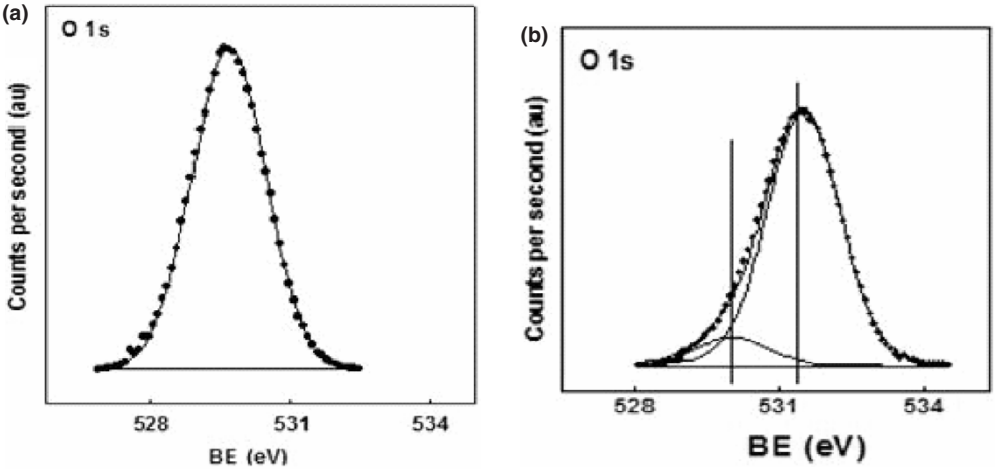

Figure 8. *In situ* XPS profiles. (a) Unpromoted silver nanowires and (b) silver nanowires promoted by 0.25% of Cs after oxidation at 623 K.

Table 1. Results of the catalytic activity tests for silver nanoparticles in the epoxidation of styrene at 573 K.

	Catalytic activity		
Catalyst[a]	X(%)[b]	Phe(%)[c]	SO(%)[d]
$11\%Ag^{(NW)}/\alpha\text{-}Al_2O_3$	57.6	57.5	42.5
$11\%Ag^{(NC)}/\alpha\text{-}Al_2O_3$	56.9	68.6	31.4
$11\%Ag^{(NP)}/\alpha\text{-}Al_2O_3$	57.5	69.2	30.8
$11\%Ag^{(NW)}/CaCO_3$	93.1	74.4	24.6
$11\%Ag^{(NW-0.25\%Cs)}/\alpha\text{-}Al_2O_3$	94.6	44.4	55.6
$11\%Cu^{(NS)}/\alpha\text{-}Al_2O_3$	0.5	Traces	Traces

[a] NW – silver nanowires; NC – silver nanocubes; NP – silver nanopolyhedra; NS – copper nanospheres.
[b] Conversion (X) of styrene.
[c] Selectivity to phenylacetaldehyde (Phe%).
[d] Selectivity to styrene oxide (SO%). O_2: C_8H_8 molar ratio of 50.

Indeed there is an intimate correlation between the XPS and TPR results. From figure 8, the O1s peak signal observed for the unpromoted silver nanowires was around 529.7 eV. However, when cesium was added the O1s peak showed two components, the major one at around 531.5 eV and a less intense one at around 529.8 eV. The deconvoluted peak of the O1s component with a binding energy value of around 531.5 eV represents around 90% for the sample oxidized at 623 K. These O-species have been ascribed to O_β (531.5 eV) and O_γ species (529.8 eV) [35, 40].

Table 1 shows the catalytic activity results of the different shape silver nanoparticles in the epoxidation of styrene. A blank test run with the α-Al_2O_3 and $CaCO_3$ support showed no conversion of styrene at the reaction temperature (523 K). The pure silver nanowire catalyst (11% $Ag^{(NW)}/\alpha$-Al_2O_3) showed a styrene conversion of 57.6% and a selectivity to styrene oxide of 42.5%. Silver nanopolyhedra and nanocubes supported

on α-Al_2O_3 showed similar catalytic performance compared to the silver nanowires. When $CaCO_3$ was used as support for the silver nanocubes the styrene conversion increased from 42.5 to 93.1% and the selectivity toward phenylacetaldehyde increased (74.4%). The addition of Cs on silver nanowire catalysts increased the catalytic activity. Styrene conversion of 94.6% was observed for a cesium loading of 0.25 wt.%. As is depicted in table 1, the higher catalytic activity for the cesium promoted sample compared to the unpromoted silver sample (11% $Ag^{(NW)}/\alpha$-Al_2O_3) may be a consequence of electronic effects of the cesium on the properties of the silver since alkaline metals may act as electron donator increasing the electron density of Ag and hence affecting their reducibility. As is well known, Cs is an electron-donating element, which can reduce the electrophilicity of oxygen species adsorbed on Ag surface, decreasing the activation energy of epoxidation and leading to the formation of selective oxidation product such as styrene oxide (SO) [44]. The addition of cesium increases the peak signal and reduces also the temperature of reduction (T_{max}) when compared with the unpromoted silver nanowire catalyst. In line with these observations, the shift of peak maxima (T_{max}) in the TPR analysis to lower temperatures for the cesium promoted silver nanowire sample may clearly indicate the formation of more reducible silver species compared with the unpromoted sample. In fact since repetitive redox cycles occur during the selective oxidation of styrene it can also be suggested that the low catalytic activity observed for the unpromoted silver nanowire sample may be due to the fact that the oxidation–reduction cycle is more difficult than for the cesium promoted silver nanowire samples. So, cesium promotion may play an important role in increasing the catalytic activity as well as preventing the isomerization route to phenylacetaldehyde. Additionally it also seems that there is a direct relationship between the epoxidation performance of the silver catalyst and the O1s signal associated with O_β specie. The O_β specie seems to be critical for the activation of silver for the styrene epoxidation.

In contrast to the silver nanoparticle catalysts, the copper nanospheres catalyst (11% $Cu^{(NS)}/\alpha$-Al_2O_3) showed negligible catalytic activity for the same reaction conditions experimented for silver catalysts. These results are also consistent with previous studies, which have shown that when the oxygen-metal bond is too strong, the catalytic activity as well as the formation of selective products such as epoxides is thermodynamically impossible [45]. By XRD it has been observed that during the reaction the silver was in metallic form, while for copper catalysts, CuO and Cu_2O were the detected phases. This indicates a stronger interaction between oxygen and the metal for copper than for silver. So, the unique characteristic of the silver in contrast to copper catalysts in the epoxidation of non-allylic olefins such as the case of styrene is founded on its ability to dissociatively adsorb oxygen, which is weakly bound on the metal surface. Previous studies showed that the difference in the relative stabilities of different oxygen species on different metal surfaces plays a strong role in the catalytic performance [46].

3.4. *Propene epoxidation using the metal nanoparticles*

The propene epoxidation was investigated over gold nanoparticles and copper nanoparticles obtained by procedure B. These particles were supported on TiO_2 spheres obtained by the Stöber method. Figure 9(a) and (b) shows the SEM and TEM

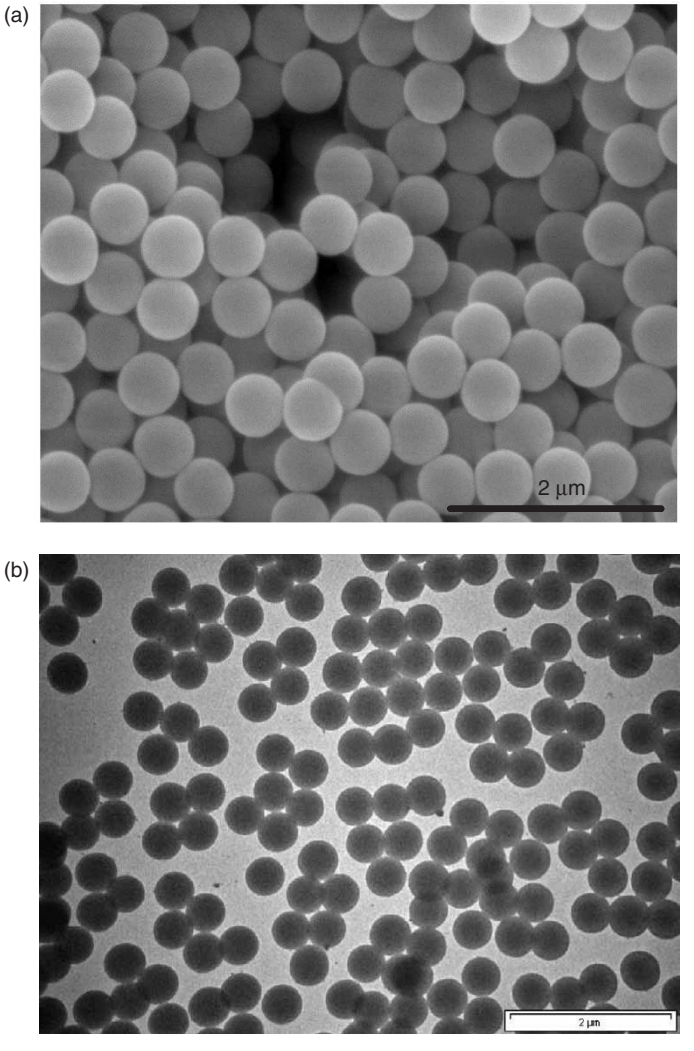

Figure 9. Monodispersed TiO_2 spheres prepared by the Stöber method. (a) SEM and (b) TEM images.

micrograph of the as-synthesized titania spheres, respectively. The TiO_2 microspheres have an average diameter of around 500 nm. The amine capped Au nanoparticle toluene solution was then mixed with the TiO_2 microspheres. The solvent was evaporated slowly and the samples were calcined in air at 623 K for 4 h in order to remove the amine. The Au content in the titania microsphere was measured to be approximately 1 wt.% by inductively coupled plasma atomic emission spectrometry (ICP-AES). The morphology of the Au nanoparticles supported on the TiO_2 microspheres before and after calcination at 623 K is depicted in figure 10(a) and (b), respectively. The TEM images show that the Au nanoparticles are isolated and well dispersed on the support (1% Au/TiO_2). The supported gold nanoparticles have a

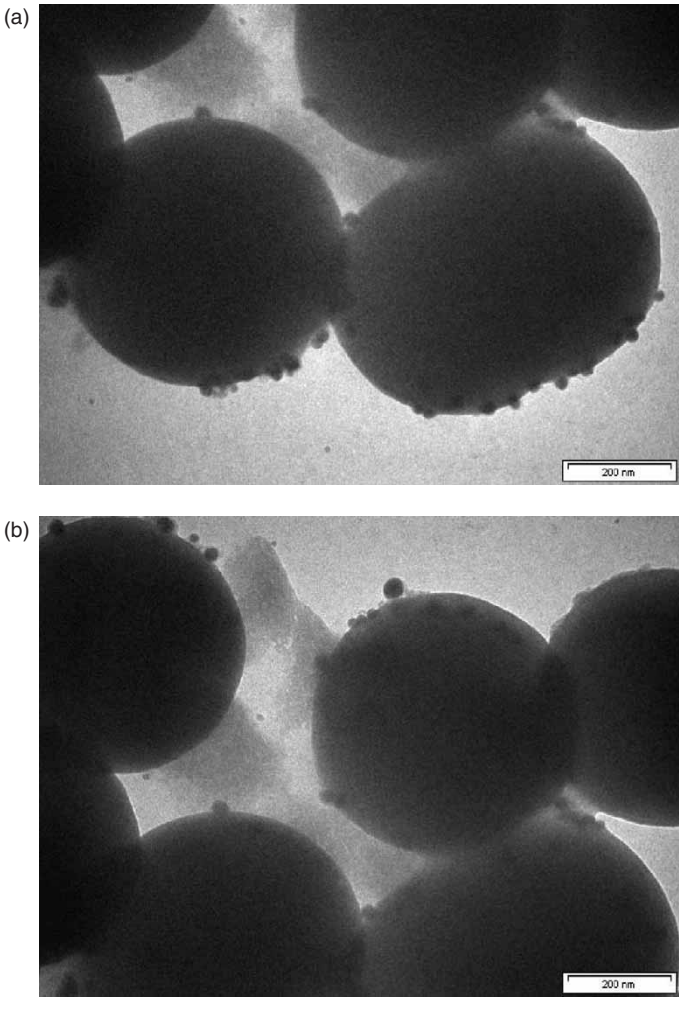

Figure 10. TEM image of gold nanoparticles coating the TiO_2 spheres. (a) Before and (b) after calcinations at 623 K.

narrow size distribution (particle size around 10 nm) with only modest sintering after calcination. The same approach was adopted for the Cu nanoparticles (synthesized by procedure B) to support on TiO_2 spheres (1% Cu/TiO_2).

For comparison the silver nanowires and copper nanospheres obtained by the polyol process were supported on TiO_2 (anatase). The total metal content was 1 wt.%. These catalysts are labelled as 1% $Ag^{(NW)}/TiO_2$ and 1% $Cu^{(NS)}/TiO_2$.

The propene epoxidation reaction in the gas phase using N_2O and O_2 as oxidants was studied using these catalysts. The main obtained products were acrolein, acetone, ethanal, propanal, propene oxide and total combustion products (H_2O and CO_2). A loss in the catalytic activity was observed during the catalytic study. This deactivation, however, was completely reversible and the activity was completely

Table 2. Effect of the temperature on the performance of the metal nanoparticles in the epoxidation of propene with nitrous oxide[a].

Catalyst	*T*(K)	X(%)	Y_{PO}(%)	ACR(%)[c]	Others[d]
1% Au/TiO_2	593	1.69	22.2	40.0	51.2
	613	2.16	15.2	49.0	42.0
	633	2.52	16.4	41.0	53.1
1% Cu/TiO_2	593	1.44	29.3	10.5	80.1
	613	1.68	29.1	14.8	72.8
	633	1.80	23.0	18.9	67.1
1% $Cu^{(NS)}/TiO_2$	593	0.06	12.1	33.3	55.2
	593[b]	1.51	4.35	74.8	22.3
	613	1.10	3.52	54.0	33.7
	633	1.41	–	71.3	28.7
1% $Ag^{(NW)}/TiO_2$	593	–	–	–	–
	593[b]	1.22	–	77.7	22.3
	613	0.01	–	79.1	20.9
	633	0.02	–	75.0	25.0

X: Conversion of propene (%). Y_{PO}: yield to propene oxide.
[a] 10% N_2O, 10% H_2, 10% C_3H_6 in argon (vol.%).
[b] 10% O_2, 10% H_2, 10% C_3H_6 in argon (vol.%).
[c] Selectivity to acrolein (ACR%).
[d] Acetone, ethanal, propanal and CO_2. Time on stream: 20 minutes.

restored in the regeneration procedure at 573 K in oxygen/helium. Previous studies have been proposed in which the deactivation is due to consecutive oxidation of the bidentate propoxy species to carboxylates [47].

Table 2 illustrates the performance of the metal nanoparticles on the propene epoxidation. The catalytic activity was studied in the range of temperature of 593–633 K. The 1% Au/TiO_2 and 1% Cu/TiO_2 catalysts showed higher activity and yield toward propene oxide (PO) compared with 1% $Ag^{(NW)}/TiO_2$ and 1% $Cu^{(NS)}/TiO_2$. In particular, the 1% Cu/TiO_2 showed the highest yield to propene oxide. At 593 K the 1% Cu/TiO_2 catalyst showed a yield toward PO of 29.3% whereas for the 1% Au/TiO_2 catalyst the yield to PO was 22.2%. The conversion of propene for the 1% Au/TiO_2 was slight higher than for 1%Cu/TiO_2. The selectivity toward PO increased at lower reaction temperatures. In line with this study Lambert and coworkers [48] have shown that copper is an effective catalyst for propene epoxidation comparable to the gold catalyst reported by Haruta [49]. Here no propene oxide was obtained with the 1% $Ag^{(NW)}/TiO_2$ catalyst. When O_2 was used as oxidant the selectivity toward acrolein increased for all the catalysts. This was evidenced by the experiments at 593 K as depicted in table 2. Smaller copper particles (procedure B) were considerably more active and selective for epoxidation, whereas the copper nanoparticles synthesized by the polyol process (procedure A) supported on TiO_2 showed higher selectivity toward acrolein. At 593 K the copper nanoparticles supported on titania spheres (catalyst 1% Cu/TiO_2) showed a propene conversion and yield to PO of 1.44% and 29.3%, respectively. However, copper nanospheres obtained by the polyol process supported on titania (catalyst 1% $Cu^{(NS)}/TiO_2$) showed a propene conversion and a yield to PO of 0.06% and 12.1%, respectively.

Consequently, the silver nanowire catalysts and copper nanosphere catalysts obtained by the polyol process were not effective in the propene epoxidation reaction when compare with Au and Cu nanoparticles obtained by the other procedures. According to these results, a key parameter for the catalytic activity in propene epoxidation seems to be the size of the metal particles. Indeed, Haruta and coworkers have shown that gold particles of 2–5 nm in size seem to be optimal for propene epoxidation. Particles that are too large have low activity and relatively higher selectivity toward total combustion [49–51].

4. Conclusions

Polyol synthesis was employed to produce Ag and Cu nanoparticles with well-defined shapes (wires/rods, cubes, polyhedra and spheres). The morphology of the silver nanostructures was strongly influenced by the $AgNO_3$ molar ratio, temperature and time in the reaction of the polyol process. Silver nanocubes were obtained when the $AgNO_3$ was increased from 1.5 to 3. Nanopolyhedra were obtained submitting the nanocubes for a longer time in the reaction mixture. Spherical copper nanoparticles were obtained in the polyol process. Styrene epoxidation by oxygen was carried out with the different silver nanostructure catalysts. The catalytic performance of the silver nanostructures (nanowires, nanocubes and nanopolyhedra) was similar. Addition of CsOH to the silver nanowires significantly improves conversion of styrene and the selectivity to SO. $CaCO_3$ used as support for the silver nanocubes increased the activity and the selectivity toward the phenylacetaldehyde compared to the α-A_2O_3 support. TPR experiments indicated that the cesium affected the reducibility of the silver. Moreover, correlating the epoxidation of styrene with the XPS analytic results, it was also found that there is a direct relationship between the epoxidation performance of catalyst and O1s signal associated with the O_β specie. The presence of O_β species seems to be critical for the catalytic activity of silver catalysts in this reaction. The copper nanosphere catalyst ($11\%Cu^{(NS)}/TiO_2$) showed negligible activity to the epoxidation of styrene.

In propene expoxidation by nitrous oxide, the 1% Au/TiO_2 and 1% Cu/TiO_2 catalysts showed the highest catalytic performance compared with the silver nanowires and copper nanospheres obtained by the polyol process. In particular, the 1% $Ag^{(NW)/}TiO_2$ showed negligible yield to PO. Besides, based on our experimental conditions, the 1% Cu/TiO_2 catalyst was more selective to PO than the 1% Au/TiO_2. Furthermore, the selectivity to propene oxide (PO) decreased as the reaction temperature increased. The selectivity to acrolein increased under more severe oxidant conditions such as molecular oxygen as oxidant or higher reaction temperatures. The size of the metal particle seems to be crucial in the epoxidation of propene.

Acknowledgements

This work was supported by the Ministerio de Ciencia y Tecnologia (Spain) under Projects PETRI 95-0801.OP and CTQ2006-08196/PPQ.

References

[1] W.P. Halperin. Quantum size effects in metal particles. *Rev. Mod. Phys.*, **58**, 533 (1996).
[2] G. Schimid. Large clusters and colloids Metals in the embryonic state. *Chem. Rev.*, **92**, 1709 (1992).
[3] A. Henglein. Small-particle research: physicochemical properties of extremely small colloidal metal and semiconductor particles. *Chem. Rev.*, **89**, 1861 (1989).
[4] M.R. Bomer, L.G. Fokkin, C. Schonenberger, B.M.I. van der Zande. Schonenberge aqueous gold sols of rod-shaped particles. *Phys. Chem. B*, **101**, 852 (1997).
[5] S.R. Nicewarner, R.G. Freeman, D.B. Reiss, L. He, D.J. Pena, I.D. Walton, R. Cromer, C.D. Keating, M.J. Natan. Submicrometer metallic barcodes. *Science*, **294**, 137 (2001).
[6] K. Esumi, K. Matsuhisa, K. Torigoe. Preparation of rodlike gold particles by UV irradiation using cationic micelles as a template. *Langmuir*, **11**, 3285 (1995).
[7] C.J. Murphy, N.R. Jana. Controlling the aspect ratio of inorganic nanorods and nanowires. *Adv. Mater.*, **14**, 80 (2002).
[8] Y.G. Sun, Y.N. Xia. Star-shaped thieno-[3,4-b]-pyrazines: a new class of red-emitting electroluminescent materials. *Adv. Mater.*, **14**, 823 (2002).
[9] Y.Y. Yu, S.S. Chang, C.L. Lee, C.R.C. Wang. Gold nanorods: electrochemical synthesis and optical properties. *J. Phys. Chem. B*, **101**, 6661 (1997).
[10] S.S. Chang, C.W. Shih, C.D. Chen, W.C. Lai, C.R.C. Wang. The shape transition of gold nanorods. *Langmuir*, **15**, 701 (1999).
[11] Z.L. Wang, M.B. Mohamed, S. Link, M.A. El-Sayed. Crystallographic facets and shapes of gold nanorods of different aspect ratios. *Surf. Sci.*, **440**, L809 (1999).
[12] Y. Sun, Y. Xia. Shape-controlled synthesis of gold and silver nanoparticles. *Science*, **298**, 2176 (2002).
[13] G. Gao. *Nanostructures and Nanomaterials: Synthesis, Properties and Applications*, Imperial College Press, London (2004).
[14] M.P. Pilene. Fabrication and properties of nanosized material made by using colloidal assemblies as templates. *Cryst. Res. Technol.*, **33**, 1155 (1998).
[15] W. Stöber, A. Fink. Controlled growth of monodisperse silica spheres in the micron size range. *J. Colloid. Interface Sci.*, **3**, 571 (1948).
[16] R.A. van santen, H.P.C. Kuipers. The mechanism of ethylene epoxidation. *Adv. Catal.*, **35**, 265 (1987).
[17] W.M.H. Sachtler, C. Backx, R.A. Van Santen. Study of the mechanism for NO_x reduction with ethanol on γ-alumina supported silver. *Cat. Rev. Sci. Eng.*, **23**, 127 (1981).
[18] M.A. Barteau, R.J. Madix. Low-pressure oxidation mechanism and reactivity of propylene on silver(110) and relation to gas-phase acidity. *J. Am. Chem. Soc.*, **105**, 344 (1983).
[19] T. Hayashi, K. Tanaka, M. Haruta. Selective vapor-phase epoxidation of propylene over Au/TiO_2 catalysts in the presence of oxygen and hydrogen. *J. Catal.*, **178**, 566 (1998).
[20] V.N. Parmon, G.I. Panov, A. Uriarte, A.S. Noskov. Nitrous oxide in oxidation chemistry and catalysis: application and production. *Catal. Today*, **100**, 115 (2005).
[21] G. Ramis, G. Busca, F. Bregani. Catalytic abatement of NO_x: Chemical and mechanistic aspects. *Gazz. Chim. Ital.*, **122**, 79 (1992).
[22] V. Duma, D. Hönicke. Gas phase epoxidation of propene by nitrous oxide over silica-supported iron oxide catalysts. *J. Catal.*, **191**, 93 (2000).
[23] R.J. Chimentão, I. Cota, A. Dafnov, F. Medina, J.E. Sueiras, J.L.G.F. Fuente, J.L.G. Fierro. Synthesis of silver–gold alloy nanoparticles by a phase transfer system. *J. Mater. Res.*, **21**, 105 (2006).
[24] Y. Sun, Y. Xia. Triangular nanoplates of silver: synthesis, characterization, and use as sacrificial templates for generating triangular nanorings of gold. *Adv. Mater.*, **15**, 695 (2003).
[25] C.J. Murphy, N.R. Jana. Controlling the aspect ratio of inorganic nanorods and nanowires. *Adv. Mater.*, **14**, 80 (2002).
[26] A.W. Vere. *Crystal Growth: Principles and Progress*, Plenum, New York (1987).
[27] B.D. Cullity, S.R. Stock. *Elements of X-Ray Diffraction*, Prentice-Hall, Upper Saddle River (2001).
[28] D. Briggs, M.P. Seah. *Practical Surface Analysis, Auger and X-Ray Photoelectron Spectroscopy*, John Wiley, Chichester (1990).
[29] A.Q. Wang, J.H. Liu, S.D. Lin, T.S. Lin, C.Y. Mou. A novel efficient Au–Ag alloy catalyst system: preparation, activity, and characterization. *J. Catal.*, **233**, 186 (2005).
[30] R.L. Penn, J.F. Banfield. Banfield, imperfect oriented attachment: dislocation generation in defect-free nanocrystals. *Science*, **297**, 237 (2002).
[31] S. Link, C. Burda, M.B. Mohamed, B. Nikoobakht, M.A. El- Sayed. New transient absorption observed in the spectrum of colloidal CdSe nanoparticles pumped with high-power femtosecond pulses. *J. Phys. Chem. B*, **103**, 1165 (1999).
[32] P.V. Kamat. Photophysical, photochemical and photocatalytic aspects of metal nanoparticles. *J. Phys. Chem. B*, **106**, 7729 (2002).

[33] I. Lisiecki, F. Billoudet, M.P. Pileni. Control of the shape and the size of copper metallic particles. *J. Phys. Chem.*, **100**, 4160 (1996).
[34] A.J. Nagy, G. Mestl. High temperature partial oxidation reactions over silver catalysts. *Appl. Catal.*, **188**, 337 (1999).
[35] A.J. Nagy, G. Mestl, R. Schlögl. The role of subsurface oxygen in the silver-catalyzed, oxidative coupling of methane. *J. Catal.*, **188**, 58 (1998).
[36] D. Herein, A. Nagy, H. Schubert, G. Weinberg, E. Kitzelmann, R. Schlögl. The reaction of molecular oxygen with silver at technical catalytic conditions: bulk structural consequences of a gas–solid interface reaction. *Z. Phys. Chem.*, **197**, 67 (1996).
[37] A.J. Nagy, G. Mestl, D. Herein, G. Weinberg, E. Kiltzelmann, R. Schlögl. The correlation of subsurface oxygen diffusion with variations of silver morphology in the silver–oxygen system. *J. Catal.*, **182**, 417 (1999).
[38] G.A. Somorjai. *Introduction to Surface Chemistry and Catalysis*, John Wiley, New York (1994).
[39] W.X. Li, C.S. Stampfl, M. Scheffler. Subsurface oxygen and surface oxide formation at Ag(111): a density-functional theory investigation. *Phys. Rev. B*, **67**, 045408 (2003).
[40] X. Bao, M. Muhler, T. Scedel-Niedrig, R. Schlögl. Interaction of oxygen with silver at high temperature and atmospheric pressure: a spectroscopic and structural analysis of a strongly bound surface species. *Phys. Rev. B*, **54**, 2249 (1996).
[41] A. Nagy, G. Mestl, T. Rüle, G. Weinberg, R. Schlögl. The dynamic restructuring of electrolytic silver during the formaldehyde synthesis reaction. *J. Catal.*, **179**, 548 (1998).
[42] G.I.N. Waterhouse, G.A. Bowmaker, J.B. Metson. Influence of catalyst morphology on the performance of electrolytic silver catalysts for the partial oxidation of methanol to formaldehyde. *Appl. Catal.*, **214**, 36 (2003).
[43] XPS International fundamental XPS data tables, www. xpsdata.com
[44] J.P. Dum, H.G. Stanger Jr, I.E. Wachs. Dynamic behavior of supported vanadia catalysts in the selective oxidation of ethane: in situ Raman, UV-Vis DRS and reactivity studies. *Catal. Today*, **301**, 51 (1999).
[45] W.M.H. Sachtler, C. Backx, R.A. Van Santen. Suppressed hydrogen chemisorption of zeolite encaged metal clusters: discrimination between theoretical models on the basis of Ru/NaY. *Cat. Rev. Sci. Eng.*, **23**, 127 (1981).
[46] H. Nakatsuji, Z.M. Hu, H. Nakai. Theoretical studies on the catalytic activity of Ag surface for the oxidation of olefins. *Int. J. Quan. Chem.*, **65**, 839 (1997).
[47] T.A. Nijhuis, T. Visser, B.M. Weckhuysen. Mechanistic study into the direct epoxidation of propene over Gold/Titania catalysts. *J. Phys. Chem. B*, **109**, 19309 (2005).
[48] O.P.H. Vaughan, G. Kryakou, N. Macleod, Mintcho Tikhov, R.M. Lambert. Copper as a selective catalyst for the epoxidation of propene. *J. Catal.*, **236**, 401 (2005).
[49] M. Haruta, M. Date. Advances in the catalysis of Au nanoparticles. *Appl. Catal.*, **222**, 128 (2001).
[50] P. Harriott. The oxidation of ethylene using silver on different supports. *J. Catal.*, **21**, 56 (1971).
[51] M. Jarjoui, B. Moravec, P.C. Granelle, S.J. Teichner. Influence of the dispersion of silver on the activity and on the selectivity of Ag-SiO_2 catalysts for ethylene oxidation.1. Preparation and characterization of catalyst. *J. Chim. Phys.*, **75**, 1061 (1978).